applied optics

In vivo 3D imaging of the human tympanic membrane using a wide-field diagonal-scanning optical coherence tomography probe

Kibeom Park,[1,2,†] Nam Hyun Cho,[3,4,†] Jeong Hun Jang,[5] Sang Heun Lee,[6] Pilun Kim,[2] Mansik Jeon,[1] Stephen A. Boppart,[7,8] Jeehyun Kim,[1,10] and Wonggyu Jung[9,*]

[1]School of Electronics Engineering, Kyungpook National University, Daegu 702-701, South Korea
[2]Oz-tec Co., Ltd., Daegu 702-701, South Korea
[3]Eaton-Peabody Laboratories, Massachusetts Eye and Ear Infirmary (MEEI), 243, Charles Street, Boston, Massachusetts 02114, USA
[4]Department of Otology and Laryngology, Harvard Medical School, 243, Charles Street, Boston, Massachusetts 02114, USA
[5]Department of Otolaryngology, Ajou University School of Medicine, 164 World cup-ro, Yeongtong-gu, Suwon, South Korea
[6]Department of Otorhinolaryngology-Head and Neck Surgery, Daegu Veterans Hospital, Daegu 704-802, South Korea
[7]Department of Electrical and Computer Engineering, University of Illinois at Urbana-Champaign, Urbana, Illinois 61801, USA
[8]Beckman Institute for Advanced Science and Technology, Urbana, Illinois 61801, USA
[9]Ulsan National Institute of Science and Technology, School of Nano-Bioscience and Chemical Engineering, 689-798, South Korea
[10]e-mail: jeehk@knu.ac.kr
*Corresponding author: wgjung@unist.ac.kr

Received 14 October 2016; revised 31 January 2017; accepted 2 February 2017; posted 2 February 2017 (Doc. ID 278740); published 1 March 2017

A wide-field optical coherence tomography (OCT) probe was developed that adapts a diagonal-scanning scheme for three-dimensional (3D) *in vivo* imaging of the human tympanic membrane. The probe consists of a relay lens to enhance the lateral scanning range up to 7 mm. Motion artifacts that occur with the use of handheld probes were found to be decreased owing to the diagonal-scanning pattern, which crosses the center of the sample to facilitate entire 3D scans. 3D images could be constructed from a small number of two-dimensional OCT images acquired using the diagonal-scanning technique. To demonstrate the usefulness and performance of the developed system with the handheld probe, *in vivo* tympanic membranes of humans and animals were imaged in real time.

OCIS codes: (110.4500) Optical coherence tomography; (170.4940) Otolaryngology; (170.4500) Optical coherence tomography.

https://doi.org/10.1364/AO.56.00D115

1. INTRODUCTION

The acousto-mechanical transduction process of hearing is delivered through a complicated anatomical structure. The middle ear consists of the tympanic membrane (TM), ossicles, and the middle ear cavity. The main role of the middle ear is to convert external acoustic signals, which are collected from the external auditory canal, into a mechanical vibration signal. However, when these fine structures are exposed to the external environment, bacterial infections can occur, and can result in structural damage [1]. Damage from otitis media (OM) is the main cause of conductive hearing loss, and hearing loss is currently classified as one of the three most common critical illnesses (hearing loss, heart disease, and arthritis) [2]. The TM is the first site to examine for the presence of any ear-related diseases, and the human TM has a diameter of approximately 7–10 mm. Widely accepted diagnostic methods, such as otoscopy and endoscopy, can only image the surface layer of the TM [3,4]. In recent years, optical coherence tomography (OCT) has been actively performed in the ear, nose, and throat as a diagnostic technique for the identification of various diseases, since it is capable of tomographic imaging [5–8]. OCT is a noninvasive, high-resolution (1–15 μm), and depth-resolved cross-sectional imaging technology that performs low-coherence interferometry utilizing light from a near-infrared wavelength-range light source [9–11].

OCT imaging is commonly performed by transversely scanning a focused optical beam linearly across the tissue, and that has been used in various fields [12,13]. In otorhinolaryngology, the correlation of the scanning angle and the physical distance between the sample and the scanning mirror are important. This is particularly important when imaging the TM because the scanning range is limited to 2–3 mm as a result of the distal exit diameter of the ear speculum tip and the ear canal. Due to these technical constraints, imaging the entire TM is

challenging, and it may decrease the reliability of the diagnostic evaluation. Furthermore, these scanning methods require a large amount of two-dimensional (2D) data, which reduces the system acquisition and display rates. When these system rates are reduced, it subsequently becomes difficult to obtain reliable three-dimensional (3D) images, because of the image artifacts associated with the movement of both the patient and operator [14].

In this paper, a diagonal-scanning probe for TM imaging and OM diagnostics using a relay lens configuration is proposed. It is found that implementation of the diagonal-scanning method improves the size of the scanning area by approximately 3.5 times compared to that of a linear scanning system without a relay lens. Further, the diagonal-scanning method significantly improves the data acquisition rate, as the sampling numbers are reduced by at least two times compared to those of conventional rectangular raster-scanning methods. Moreover, the motion artifacts were minimized by implementing the Compute Unified Device Architecture (CUDA) process, which enhances the image acquisition speed.

2. MATERIALS AND METHOD

A. Instrumentation

A schematic diagram of the spectral domain (SD)-OCT system is shown in Fig. 1(a). A 12-bit complementary metal-oxide semiconductor (CMOS) line scanning camera (Sprint spL4096-140 k, Basler AG) with a 70,000-line/s effective line rate at a 4,096-pixel mode was used as the detector in the SD-OCT system. The spectrometer was calibrated following a method reported by Jeon *et al.* [15]. Combined with a superluminescent diode (SLED; $\lambda_o = 850$ nm, $\Delta\lambda = 65$ nm; Superlum) as a light source, B-mode scanning was performed using a two-axis galvanometer scanner (GVS002, Thorlabs) at the back focal plane of the objective lens in the sample path.

The parameter angle, lateral resolution, scanning range, and tip size were considered in the probe design. Figure 1(b) shows the design of the lens combination, which uses a relay lens and a focusing lens to obtain a wide scanning range. The collimated beam from the galvanometer scanning mirrors was directed through the relay lenses (Lens 1 and Lens 2) to the focusing lens (Lens 3). The scanning angle between the end of the scanning range and the central point is represented by θ. The probe was designed to have a lateral resolution less than 15 μm and a scanning range more than 7 mm. To achieve these parameters, the lateral resolution and the scanning range were simulated by varying the length of the focal length of Lens 1 (f1) and the Lens 3 focal length (f3). The focal length of each lens affects the lateral resolution, scanning angle, and beam size. To simplify the simulation, a ratio of f3 to the Lens 2 focal length (f2) was applied instead of using the f2 and f3 values separately.

B. Simulation

Figure 1(c) shows the lateral resolution values with respect to the ratio of f2 to f3 for f1 values of 10, 20, 30, and 40 mm. The lateral resolution of the system increased when f1 was reduced and the ratio of f3 to f2 was increased. However, due to the length limitation between the scanning mirror and Lens 1, f1 was finally fixed at 20 mm. The incident beam size of

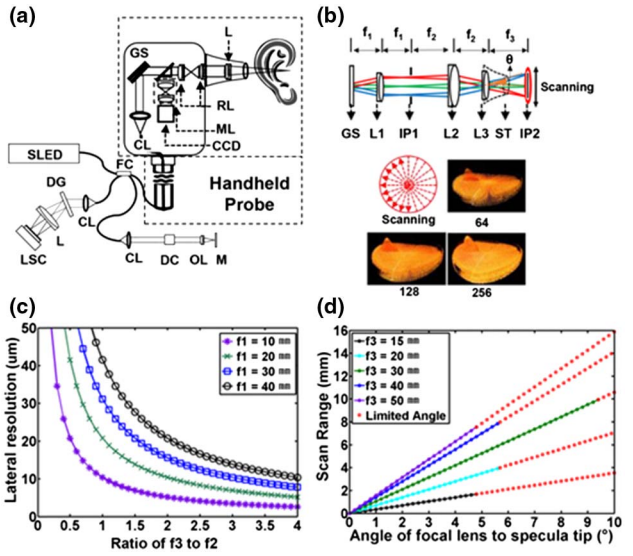

Fig. 1. (a) Schematic diagram of the spectral domain (SD)-OCT system. (b) Schematic of the OCT probe based on a relay lens and 3D reconstructions according to sampling numbers (64, 128, 256). (c) Simulated lateral resolutions for the OCT as a ratio of the focal length of Lens 3 (f3) to the focal length of Lens 2 (f2); each colored line shows the value of the focal length of Lens 1 (f1). (d) Simulated scanning range according to the scanning angle (θ) from the center of Lens 3 to the edge of the specula tip for different f3. The red lines indicate a limited angle. Abbreviations: CL, collimator; DC, dispersion compensation unit (hardware-based dispersion compensation unit was connected to the reference arm path to compensate the dispersion); DG, diffraction grating; FC, fiber coupler; GS, galvanometer scanners; L, lens; LSC, line-scanning camera; ML, magnifier lens; M, mirror; OL, objective lens, CCD, charge-coupled device, FL, focal length, PC, polarization controllers; RL, relay lens; ST, specula tip; SLED, superluminescent diode.

the collimator was assumed to be 1.5 mm. To miniaturize the probe and to obtain a 15 μm lateral resolution, the ratio of f3 to f2 was set to 1.5.

Figure 1(d) shows the maximum scanning range with respect to propagation without light loss. From the numerical calculations, the optimum f3 to achieve a scanning range of 10 mm was 30 mm. However, f3 was set to 50 mm owing to the limitation imposed by the ear canal length and the specula tip diameter. Therefore, the maximum scanning range and angle were extended to 7 mm and 4°, respectively.

By considering the probe design as well as the results of the above simulation, f1 was set to 20 mm. In addition, f2 and f3 were set to 35 mm and 50 mm, respectively, yielding a ratio of 1.5 between f2 and f3. The given parameters (f1 : 20 mm, ratio of f3 to f2 : 1.5) were used to calculate f3, considering the ear specula tip and the distance of the TM from the system.

In many OCT applications, image acquisition is performed using a stable beam-delivery system on a stably positioned sample. Thus, 3D image acquisition can be readily performed using a standard raster-scanning method. However, for the system developed in this study, images are acquired using a handheld probe, and the biological tissue (e.g., the middle ear and TM) cannot be easily stabilized during longer periods of image

acquisition. Accordingly, 3D image acquisition of the middle ear using raster scanning is not as reliable or accurate, as the initial position of the 3D scanning data can be easily misregistered due to the movement of the handheld probe or the human body. However, using the radial-scanning method proposed here, the exact center point of the diagonal scans can be readily fixed to a particular target point on the TM, and can be maintained during diagonal scanning. This target point should be considered as the center of the cylindrical volume of image data. If a change in this central target point is detected, a mismatch between the exact center point and the scanned data, due to motion artifacts, can be easily identified. Thus, the diagonal-scanning method (which resembles spokes on a bicycle wheel) is more effective and reliable than the rectangular raster-scanning method, as motion artifacts affecting the accuracy of the raster-scanning method cannot be readily identified owing to the absence of a center target point within the image data. In this study, it is confirmed that motion artifacts are minimized with the use of this center target point. Therefore, 3D images with less motion artifact can be acquired. This diagonal-scanning method is also more efficient when time-consuming 3D scanning is performed, because the path of each cross-sectional B-mode image always crosses the center of the sample in diagonal scanning. Also, the diagonal-scanning method can reduce the number of B-scan images, though we sacrificed lateral resolution by decreased sampling number, and decrease the required scanning time for volume acquisition. With an imaging acquisition and display speed of 100 fps from our GPU-based system, real-time 3D imaging is practical [16]. Combined use of the diagonal-scanning method and the GPU-based system have the benefits of both, enabling 3D volume imaging and reducing the motion artifacts associated with 3D volume acquisition.

3. RESULTS AND DISCUSSION

Figure 2 shows an *in vivo* image of a human TM, with a 2-mm image taken using the conventional rectangular raster-scanning method and a mounted charge-coupled device (CCD) camera, and a 7 mm wide-field image obtained using the diagonal-scanning method. The inset images in the square boxes in the bottom part of Figs. 2(a) and 2(b) are of a ruler indicating the real scanning range; each black pair represents 0.5 mm. In addition, the geometric distortion artifact arising due to the nontelecentric scanning of the sample was corrected through indexing, so as to flatten the curved part of the distorted image. The imaging area was increased to obtain further lateral information about the TM of the human middle ear. Figure 2(c) shows OCT and camera images of adhesive OM, with the latter being taken using the CCD camera built into the handheld probe, while Fig. 2(d) shows OCT and CCD camera images of a case of chronic OM. Each image, with a size of 1024 × 500 pixels, was acquired in real time in 10 ms.

Figure 3 shows *in vivo* OCT and CCD images of a perforation in a human TM. From the 3D volumetric OCT data, 2D cross-sectional OCT images are extracted and shown in Figs. 3(c)–3(e). The green circle in Figs. 3(a) and 3(b) represents the diagonal-scanning range, while the green dotted arrows indicate the 0°, 45°, and 90° scanning directions.

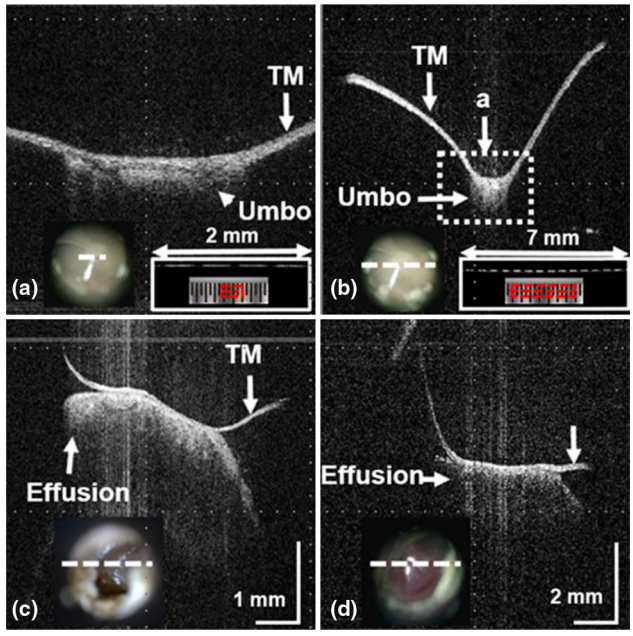

Fig. 2. 2D *in vivo* OCT images of a human TM, with (a) a 2 mm scanning range using the conventional linear scanning method, and (b) a 7 mm scanning range using the wide-field OCT probe. The images shown at the lower right corners in (a) and (b) represent camera images and cross-sectional images of a metal ruler. OCT and CCD camera images of an adhesive OM and a chronic OM are shown in (c) and (d), respectively.

Diagonal scanning for 3D acquisition is conducted in a clockwise rotation, according to the indicated angle values. Each diagonal scan produces a cross-sectional B-mode image and each scan is oriented radially at 0.72° separation. The positions used for Figs. 3(a) and 3(b) are indicated by the lines in each 2D image on the abnormal TM [Figs. 3(c)–3(e)].

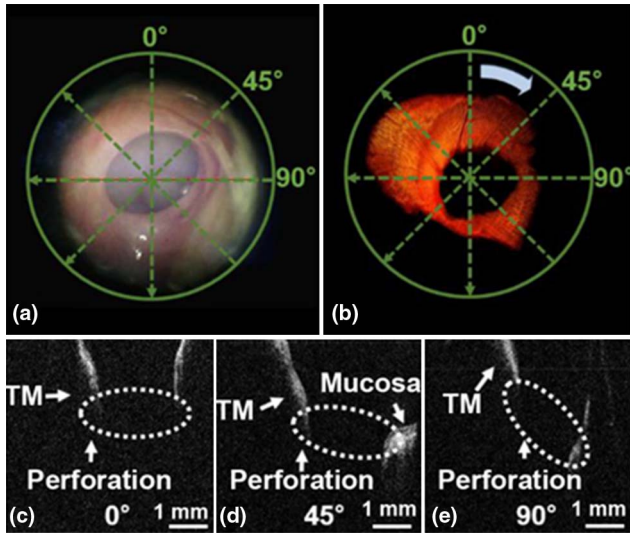

Fig. 3. *In vivo* TM image of perforation patient using diagonal scanning. (a) A CCD camera image and (b) a 3D image of a perforated TM. Two-dimensional (2D) cross-sectional OCT images are shown in (c)–(e).

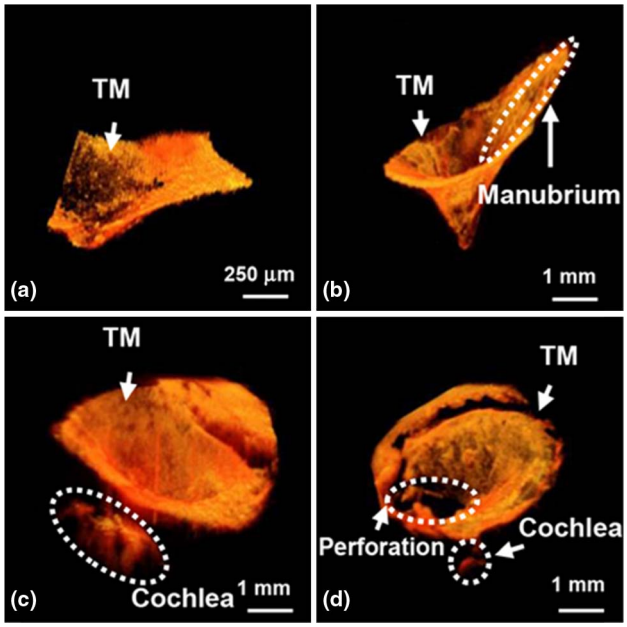

Fig. 4. 3D volumetric OCT reconstructions of guinea pig TM images. Images taken using (a) a 2 mm scanning range and the conventional 3D raster-scanning system, and (b) a 7 mm scanning range and the wide-field OCT probe, with (c) a normal and (d) a perforation.

Figure 4 demonstrates a comparison between the scanning ranges on guinea pig TM images *ex vivo*. The system was verified by acquiring images of a normal and a perforation guinea pig TM. Figures 4(a) and 4(b) are 3D volumetric images of the guinea pig TM, which are rendered in two different ranges. Figure 4(a) shows the 3D volumetric image obtained using the conventional system with a scanning range of 2 mm. Figure 4(b) is the rendered 3D volumetric image using the proposed wide-field OCT system with a scanning range of 7 mm. The visualization of the entire region of the TM verifies the enhancement of the proposed method compared to the conventional method. Figures 4(c) and 4(d) depict the normal and perforation TM regions. The volumetric image of the normal TM can be identified in Fig. 4(c) and the cochlea can be seen underneath the TM. Figure 4(d) represents the perforation TM. The exact location and the size of the perforation can be identified through the image. It is evident that the larger 7 mm scan range provides a more comprehensive view of the TM for identifying pathological features and making a diagnosis.

4. CONCLUSION

In conclusion, we have reported the development of a wide-field OCT probe that utilizes a diagonal-scanning scheme for 3D *in vivo* imaging of the human TM. The handheld probe consists of a relay lens to enhance the lateral scanning range up to 7 mm. The obtained simulation results and the ruler image captured with the new probe confirms a 3.5-fold lengthening of the lateral scanning range, from 2 to 7 mm. The diagonal-scanning method can be used to reduce motion artifacts that occur when handheld probes are used, because each individual B-mode image crosses the center of the sample when 3D scanning is being conducted. It is possible to construct a 3D image using only half the number of 2D OCT images acquired through diagonal scanning, compared to raster scanning. Subsequently, the 3D image reconstruction time can be halved by reducing the number of samples from 500 to 250. To demonstrate the usefulness and performance of the developed system with the handheld probe, human and animal TMs were imaged *in vivo* and in real time. The diagonal-scanning method can be beneficial with regard to any handheld OCT probe, as it reduces motion artifacts; it also has advantages for 3D scanning, as it reduces the number of scans required for reasonable image quality. In the future, this diagnostic tool for otolaryngology may be further improved by implementing micro-electromechanical system (MEMS)-based scanners in these handheld probes, as in earlier designs [17], by adding depth-color mapping methods to the 3D data, by rendering results with automated disease detection algorithms, and by demonstrating the value of these technologies in various clinical trials.

Funding. Ministry of Trade, Industry and Energy (MOTIE) (10047943); National Institutes of Health (NIH) (NIH/NIBIB 1 R01 EB023223); Ministry of Knowledge Economy (MKE); The Presidential Research of Ulsan National Institute of Science and Technology (UNIST) (1.120076).

†These authors contributed equally to this work.

REFERENCES

1. C. T. Nguyen, W. Jung, J. Kim, E. J. Chaney, M. Novak, C. N. Stewart, and S. A. Boppart, "Noninvasive *in vivo* optical detection of biofilm in the human middle ear," Proc. Natl. Acad. Sci. USA. **109**, 9529–9534 (2012).
2. Y. Lotfi, S. Mehrkian, A. Moossavi, and S. Faghih-Zadeh, "Quality of life improvement in hearing-impaired elderly people after wearing a hearing aid," Arch. Iran. Med. **12**, 365–370 (2009).
3. C. T. Nguyen, H. Tu, E. J. Chaney, C. N. Stewart, and S. A. Boppart, "Non-invasive optical interferometry for the assessment of biofilm growth in the middle ear," Biomed. Opt. Express **1**, 1104–1116 (2010).
4. N.-H. Cho, U.-S. Jung, H.-I. Kwon, H.-S. Jeong, and J.-H. Kim, "Development of SD-OCT for imaging the *in vivo* human tympanic membrane," J. Opt. Soc. Korea **15**, 74–77 (2011).
5. N. H. Cho, J. H. Jang, W. Jung, and J. Kim, "*In vivo* imaging of middle-ear and inner-ear microstructures of a mouse guided by SD-OCT combined with a surgical microscope," Opt. Express **22**, 8985–8995 (2014).
6. C. T. Nguyen, S. R. Robinson, W. Jung, M. A. Novak, S. A. Boppart, and J. B. Allen, "Investigation of bacterial biofilm in the human middle ear using optical coherence tomography and acoustic measurements," Hear. Res. **301**, 193–200 (2013).
7. E. W. Chang, J. T. Cheng, C. Röösli, J. B. Kobler, J. J. Rosowski, and S. H. Yun, "Simultaneous 3D imaging of sound-induced motions of the tympanic membrane and middle ear ossicles," Hear. Res. **304**, 49–56 (2013).
8. S. S. Gao, P. D. Raphael, R. Wang, J. Park, A. Xia, B. E. Applegate, and J. S. Oghalai, "*In vivo* vibrometry inside the apex of the mouse cochlea using spectral domain optical coherence tomography," Biomed. Opt. Express **4**, 230–240 (2013).
9. D. Huang, E. A. Swanson, C. P. Lin, J. S. Schuman, W. G. Stinson, W. Chang, M. R. Hee, T. Flotte, K. Gregory, and C. A. Puliafito, "Optical coherence tomography," Science **254**, 1178–1181 (1991).
10. J. Kim, B.-S. Sohn, and T. E. Milner, "Real-time retinal imaging with a parallel optical coherence tomography using a CMOS smart array detector," J. Korean Phys. Soc. **51**, 1787–1791 (2007).
11. B. Bouma, *Handbook of Optical Coherence Tomography* (Informa Health Care, 2001).

12. E. Lebed, S. Lee, M. V. Sarunic, and M. F. Beg, "Rapid radial optical coherence tomography image acquisition," J. Biomed. Opt. **18**, 036004 (2013).
13. F. C. Moura, L. V. F. Costa-Cunha, R. F. S. Malta, and M. L. R. Monteiro, "Relationship between visual field sensitivity loss and quadrantic macular thickness measured with Stratus-Optical coherence tomography in patients with chiasmal syndrome," Arq. Bras. Oftalmol. **73**, 409–413 (2010).
14. H. R. Djalilian, J. Ridgway, M. Tam, A. Sepehr, Z. Chen, and B. J. Wong, "Imaging the human tympanic membrane using optical coherence tomography *in vivo*," Otol. Neurotol. **29**, 1091–1094 (2008).
15. M. Jeon, J. Kim, U. Jung, C. Lee, W. Jung, and S. A. Boppart, "Full-range k-domain linearization in spectral-domain optical coherence tomography," Appl. Opt. **50**, 1158–1163 (2011).
16. N. H. Cho, U. Jung, S. Kim, W. Jung, J. Oh, H. W. Kang, and J. Kim, "High speed SD-OCT system using GPU accelerated mode for *in vivo* human eye imaging," J. Opt. Soc. Korea **17**, 68–72 (2013).
17. W. Jung, J. Kim, M. Jeon, E. J. Chaney, C. N. Stewart, and S. A. Boppart, "Handheld optical coherence tomography scanner for primary care diagnostics," IEEE Trans. Biomed. Eng. **58**, 741–744 (2011).